PHYSICAL REVIEW B **87**, 121402(R) (2013)

Optical conductivity of twisted bilayer graphene

C. J. Tabert and E. J. Nicol
Department of Physics, University of Guelph, Guelph, Ontario N1G 2W1, Canada and
Guelph-Waterloo Physics Institute, University of Guelph, Guelph, Ontario N1G 2W1, Canada
(Received 11 January 2013; revised manuscript received 14 February 2013; published 11 March 2013)

We calculate the finite-frequency conductivity of bilayer graphene with a relative twist between the layers. The low-frequency response at zero doping shows a flat conductivity with value twice that of the monolayer case and at higher frequency a strong absorption peak occurs. For finite doping, the low-frequency flat absorption is modified into a peak centered at zero frequency (the Drude response) accompanied by an interband edge which results from the transfer of spectral weight from interband to intraband absorption due to Pauli blocking. If the system is doped sufficiently such that the chemical potential reaches beyond the low-energy saddle point in the twisted bilayer band structure, a strong low-frequency absorption peak appears at an energy related to an effective interlayer hopping energy, which may be used to identify this parameter and confirm the existence of the saddle point which gives rise to a low-energy van Hove singularity in the electronic density of states.

DOI: 10.1103/PhysRevB.87.121402 PACS number(s): 78.67.Wj, 78.30.−j, 78.20.Ci, 81.05.ue

Graphene remains a material of considerable promise both for technological applications and for revealing unusual and unexpected physics.[1,2] Key to this enterprise is the ability to manipulate its band structure and change the Fermi level through charge doping by electrons or holes. In the former, the layering of graphene sheets in various stacking arrangements can produce very different dispersions at low energy, such as quadratic in the Bernal-stacked bilayer versus linear in the monolayer. Recently, it has been noted that layers of graphene with a rotational misorientation can give rise to surprising behavior at low energy. Indeed, for small rotational angles of a bilayer of graphene, it is predicted that the low-energy dispersion will be linear, not unlike the monolayer,[3] and a low-energy van Hove feature will also appear in the density of states.[4–6] Moreover, the Fermi velocity v_F is reduced for small rotation angles[3] until localization appears to set in.[7,8] These features have been the subject of a number of theoretical works, such as Refs. 3,7, and 9, and have been verified by experimental groups performing scanning tunneling microscopy (STM) measurements,[4–6] although controversy remains, as discussed below.

The origin of these features is found in the details of the modified energy dispersion. In twisted bilayer graphene, the Dirac cones at the K points of the Brillouin zone in one layer undergo a relative rotation to those in the other layer (as shown in Fig.1). The two Dirac cones which are slightly shifted relative to each other then overlap and the band structure is reconstructed to form a saddle point in between. The final modified band structure around the midpoint of the split Dirac point near K is illustrated in the lower part of Fig.1 for the two lowest energy bands in the model discussed here. At low energy, the slope of the linear band structure gives a Fermi velocity, which is reduced from the graphene monolayer value, and the saddle point in between produces a van Hove singularity (VHS) in the density of states at low energy. One might have naively considered the graphene sheets to have decoupled with the relative rotation, but the presence of the renormalized Fermi velocity and VHS point to a different interpretation. In spite of a growing literature on twisted bilayer graphene, there have been few experiments which have verified these unusual results. In particular, the VHS saddle point and renormalized velocity are not seen in some angle-resolved photoemission experiments (ARPES),[10] but these features are very clear in the STM,[4–6] and some ARPES measurements do confirm the VHS.[11] The predicted behavior of the Landau levels in twisted bilayer graphene[12,13] as measured through the quantum Hall effect has not been seen in rotated layers,[14] but Raman spectroscopy of the rotational-angle-dependent graphene 2D peak[15] points to the existence of the VHS in the band structure. Further experiments are required to resolve this situation, and indeed other spectroscopies should be brought to bear on this question. The interplay of theory and experiment for the dynamical conductivity of graphene and bilayer graphene has been quite successful in the past[16–35] and consequently we provide here the theoretical calculation for the dynamical conductivity of twisted bilayer graphene, illustrating how the VHS will be manifest in this experiment.

A literature has developed for modeling misorientated bilayer graphene. A popular model for describing the state of twisted bilayer graphene is the continuum model put forth by Lopes dos Santos and coworkers,[3] where the Hamiltonian is written as[12]

$$H(\boldsymbol{k}) = \begin{pmatrix} H_0(\boldsymbol{k}+\Delta\boldsymbol{K}/2) & H_\perp \\ H_\perp^\dagger & H_0(\boldsymbol{k}-\Delta\boldsymbol{K}/2) \end{pmatrix}, \quad (1)$$

with

$$H_0(\boldsymbol{k}) = \begin{pmatrix} 0 & f^*(\boldsymbol{k}) \\ f(\boldsymbol{k}) & 0 \end{pmatrix}, \quad (2)$$

where $f(\boldsymbol{k}) = \hbar v_F(k_x + ik_y)$, and

$$H_\perp^0(\boldsymbol{k}) = \tilde{t}_\perp \begin{pmatrix} 1 & 1 \\ 1 & 1 \end{pmatrix}, \quad H_\perp^\pm(\boldsymbol{k}) = \tilde{t}_\perp \begin{pmatrix} e^{\mp i\phi} & 1 \\ e^{\pm i\phi} & e^{\mp i\phi} \end{pmatrix}, \quad (3)$$

where $\phi = 2\pi/3$ and $\tilde{t}_\perp$ is an angle-dependent interlayer hopping parameter typically quoted as being between 100 and 150 meV. Here, the rotation between the layers is captured by the monolayer graphene Hamiltonian of Eq. (2), where the argument is replaced by $\boldsymbol{k} \pm \Delta\boldsymbol{K}/2$ with $\Delta\boldsymbol{K} = \boldsymbol{K} - \boldsymbol{K}_\theta$. The expansion in k is taken about the midpoint between the two shifted Dirac cones as shown in Fig. 1. The interlayer

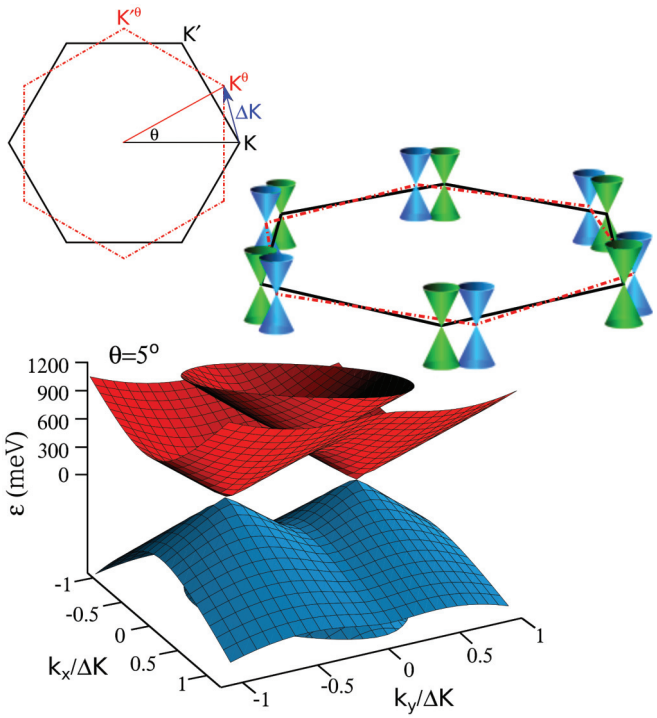

FIG. 1. (Color online) Top: The first Brillouin zones of two graphene layers where one layer is twisted (dashed red) relative to the other (solid black). The two K points, $\boldsymbol{K}$ and $\boldsymbol{K}^{\theta}$, are separated by $\Delta\boldsymbol{K}$. Middle: The relative rotation shifts the Dirac cones in one layer relative to those in the other layer, as shown schematically with blue [dark gray] and green [light gray] cones for each layer, respectively. Bottom: The low-energy band structure about the midpoint between the two Dirac cones shifted relative to the K point due to a twist angle of $\theta = 5^{\circ}$.

hopping terms represent the dominant Fourier amplitudes in the interlayer hopping as described in Ref. 3. This Hamiltonian and also *ab initio* and tight-binding methods have been employed by various authors to determine the band structure and density of electronic states. However, when including a magnetic field, some authors[12–14] have examined the Landau level structure using a low-energy effective Hamiltonian where the interlayer hopping is taken as the standard Bernal bilayer form:[12,13]

$$H_{\perp}^{\text{eff}}(\boldsymbol{k}) = \tilde{t}_{\perp}\begin{pmatrix} 0 & 0 \\ 1 & 0 \end{pmatrix}. \tag{4}$$

In zero magnetic field, this leads to an analytic expression for the low-energy dispersion given by

$$\varepsilon_{\alpha}^{2}(\boldsymbol{k}) = \tfrac{1}{2}\left[\tilde{t}_{\perp}^{2} + \varepsilon_{G}^{+2} + \varepsilon_{G}^{-2} + (-)^{\alpha}\Gamma\right],$$
$$\Gamma = \sqrt{\left(\tilde{t}_{\perp}^{2} + \varepsilon_{G}^{+2} + \varepsilon_{G}^{-2}\right)^{2} - 4\,\varepsilon_{G}^{+2}\,\varepsilon_{G}^{-2}}, \tag{5}$$

where $\alpha = 1$ and 2 and $\varepsilon_{G}^{\pm} = |f(\boldsymbol{k} \pm \Delta\boldsymbol{K}/2)|$. In these works, extensive arguments for the validity of the approximation have been given, including that the Hamiltonian remains in the same topological universality class, preserves the chirality of the wave functions, and exhibits a low-energy band structure, similar to the other methods, including split Dirac points and saddle points giving rise to the low energy VHS in the DOS. We have examined this latter form, made comparisons to the band structure of both the $G = 0$ approximation of the Lopes paper and their full numerical results presented in that paper, and find reasonable agreement between the two approaches. As the low-energy effective Hamiltonian is much more tractable for a calculation of the optical properties using Green's functions and the Kubo formula, we proceed with this effective Hamiltonian as used recently by other authors[12–14] in the spirit of capturing the essence of the effect of rotational misalignment on the finite-frequency conductivity. Note that this approach will not be appropriate for very small twist angles, where localization effects appear to set in, but should be suitable for[13] $3^{\circ} \lesssim \theta \lesssim 10^{\circ}$ which is the region in which experiments have been performed. For much larger rotation angles it has been argued[36,37] that the model of Mele[38] should be used. This latter model has been used for the calculation of magneto-optics.[39]

In Fig. 1, we show the band structure evaluated from this approach for an angle of 5°. A cut of this band structure along the line connecting the shifted Dirac cones is shown in Fig. 2. Typically the interlayer hopping $\tilde{t}_{\perp}(\theta)$ depends on angle and the specific value varies in the literature. Consequently, to make our calculation more applicable, we chose a value of $\tilde{t}_{\perp}(\theta) = 150$ meV in our approach to give a band structure with a $k = 0$ saddle-point energy and upper band minimum to approximately match the energy scales found in Ref. 6 from *ab initio* and tight-binding calculations and also confirmed therein by experimental data. With this simplified model, we capture the essential features found in the more numerical approaches: a linear dispersion at low energy at each of the two shifted Dirac points and a saddle point in the band structure at low energy. This should allow us to examine the signatures of these features in the optical properties, at least at a qualitative level.

For a calculation of the dynamical conductivity, we follow the method based on many-body Green's functions, which is shown in the work by Nicol and Carbotte[24] and Tabert and Nicol[40] for the cases of AB- and AA-stacked bilayer graphene, respectively. Specifically, we can determine the Green's function $\hat{G}(z)$ from $\hat{G}^{-1}(z) = z\hat{I} - \hat{H}$ along with its spectral representation $\hat{G}_{ij}(z) = \int_{-\infty}^{\infty} d\omega\, \hat{A}_{ij}(\omega)/[2\pi(z-\omega)]$. Using the Kubo formula,[41] where the conductivity is written in terms of the retarded current-current correlation function, we can express the real part of the finite-frequency longitudinal conductivity, at zero temperature and for photon energy Ω, as[24]

$$\sigma(\Omega) = \frac{2\,e^{2}}{\Omega}\int \mathrm{Tr}[\hat{v}_{x}\hat{A}(\boldsymbol{k},\omega+\Omega)\hat{v}_{x}\hat{A}(\boldsymbol{k},\omega)], \tag{6}$$

where

$$\int \equiv \int_{|\mu|-\Omega}^{|\mu|}\frac{d\omega}{2\pi}\int\frac{d^{2}k}{(2\pi)^{2}} \tag{7}$$

with the $\boldsymbol{k}$ integration over a region containing two shifted Dirac points. Here, μ is the chemical potential and $\hbar\hat{v}_{x} = \partial\hat{H}/\partial k_{x}$. While the conductivity shown in Eq. (6) is for σ_{xx}, it is the same for σ_{yy} and is therefore isotropic. The velocity operator brings in only the transport associated with a single graphene sheet, while the reconstructed band structure enters only through the energies in the spectral functions.

We now present the longitudinal conductivity which we obtain by a numerical evaluation of Eq. (6) with the

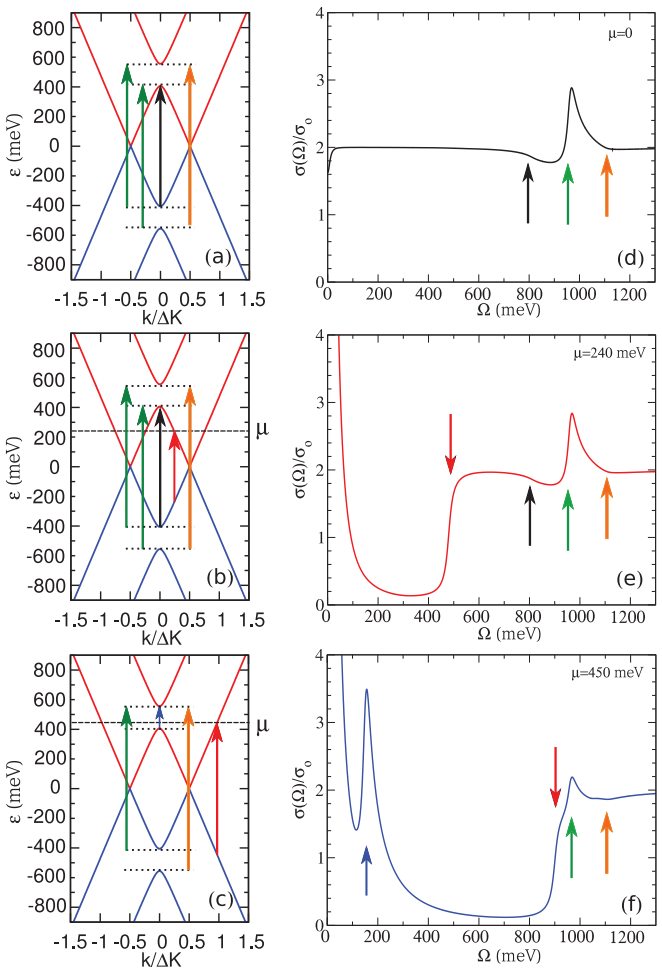

FIG. 2. (Color online) (a)–(c) Band structure along a line connecting the two K points $\boldsymbol{K}$ and $\boldsymbol{K}^{\theta}$ for $\theta = 5^{\circ}$. In each successive frame, the chemical potential is changed from (a) $\mu = 0$, (b) 240 meV, and (c) 450 meV, and various significant optical transitions are indicated which give rise to structure in the conductivity curves shown to the right. (d)–(e) The finite frequency longitudinal conductivity at zero temperature for varying chemical potential. The arrows indicate the transitions shown in the band structure to the left. $\sigma_0 = e^2/4\hbar$.

appropriate substitutions of the calculated spectral functions. The calculation follows steps similar to those already in the literature[24,40,42] and the final expressions are lengthy, so we refrain from repeating them here. For the δ functions that appear in our expressions for the spectral functions, we use the Lorentzian representation $\delta(x) \to (\eta/\pi)/[\eta^2 + x^2]$ with a broadening parameter $\eta = 7$ meV in order to do the numerical work. This broadening parameter manifests itself in the conductivity as an effective transport scattering rate of $1/\tau_{\rm imp} = 2\eta$ due to the convolution of two Lorentzians in the conductivity formula that result from the multiplication of the spectral functions.

In Fig. 2, we show the essence of the optical conductivity in twisted bilayer graphene within the model used here. Plots of the conductivity at various dopings, marked by μ, are exhibited in Figs. 2(d)–2(f). For comparison the band structure is shown at the left in Figs. 2(a)–2(c), indicating the prominent absorptive transitions identified by arrows on the plots at the right. Note that the photon momentum $\boldsymbol{q} \sim 0$ here and hence there can only be vertical transitions in this diagram. We have chosen to show our results for $\theta = 5^{\circ}$ as such an angle has been considered for other properties[9,13] and it is intermediate to the data shown in Ref. 6. The conductivity curves are scaled by $\sigma_0 = e^2/4\hbar$, which is the background conductivity of monolayer graphene.

The values of μ were chosen to span a range of behavior and to sample different regions of the band structure. In Fig. 2(d), charge neutrality is considered with $\mu = 0$. As expected, the low-energy band structure seen in Fig. 2(a) allows solely for interband transitions and a flat conductivity is found at low photon energy, reflecting the low-energy linear Dirac cones that are also found in monolayer graphene and emerge here with finite twist angle. The main difference is that there are now double the number of Dirac cones compared to graphene due to the two layers in the bilayer, and hence the universal background conductivity is $2\sigma_0$. This correlates with the linear behavior in the low-energy electronic density of states seen in STM and the monolayer behavior noted in those experiments. However, in the optics the Fermi velocity does not enter this universal background value, and as a result, the reduction in v_F with angle seen in STM experiments would not be evident here. At higher photon frequency, for $\mu = 0$, transitions between the saddle point (VHS) in the band structure to other parts of the band structure begin to occur. This results in the dip-peak structure seen around $\Omega \sim 900$ meV, for the case shown here, which is very similar to the structure calculated for unrotated Bernal-stacked bilayer graphene at charge neutrality but found, in that case, at low energy starting from $\Omega = 0$.[22] Here, the peak arises from $k = 0$ transitions involving the VHS and hence its observation should provide evidence for the VHS. As θ is increased, this structure is moved to higher energy in our model, but the low-energy behavior remains the same.

With doping away from charge neutrality to $\mu = 240$ meV, the low-energy interband transitions are blocked by the Pauli exclusion principle, and intraband transitions, facilitated by the impurity scattering rate, now give rise to a narrow Drude absorption centered about $\Omega = 0$. This Drude absorption acquires the optical spectral weight that is removed at low frequencies below $\Omega = 2\mu = 480$ meV. The dip-peak feature at higher photon energy remains the same, which would not be the case for ordinary Bernal-stacked bilayer graphene,[24] where the peak would be split into two and reduced. Thus, we find for low doping that the low-energy behavior in the dynamical conductivity will mimic the classic monolayer graphene behavior subject to a factor of two increase in the overall magnitude of the conductivity.

We turn now to a more interesting result, shown in Fig. 2(f): If $\mu = 450$ meV, the Fermi level is now above the low-energy saddle point (VHS) but below the next band in Fig. 2(c). At this doping, a new peak appears in the conductivity at low energy, marking the transition between the VHS to the second band, which in this model measures $\tilde{t}_{\perp}$. As this is a result from transitions at $k = 0$ and is at low photon energy, it should be a very robust feature in far infrared measurements. Furthermore, the peak shown in the model here is very strong. In graphene systems, the impurity scattering rate is typically small, on the order of a few meV, and hence the width of the Drude would not be expected to interfere with this feature

for intermediate rotation angle where our model applies. The spectral weight for this new VHS peak comes from the higher photon energy region in the conductivity where a number of transitions involving the VHS point in the band structure are now blocked. These are illustrated and understood by examining the arrows shown in Figs. 2(b) and 2(c). One sees that the dip-peak structure at high energy is indeed diminished in this case. Thus, we predict that there should be a signature of the existence of the controversial low-energy VHS in the optical conductivity at low photon energy with appropriate doping, which could be achieved by voltage gating or by other means, as has been done for ordinary bilayer graphene.[33,43]

Finally, not shown here, but if μ is further increased to a value which places it in the upper band (μ greater than $\sim$550 meV), then the VHS peak at low energy will be lost due to Pauli blocking. Varying μ, therefore, would provide a sensitive probe as to the energy of the saddle point VHS [$\varepsilon_{\rm VHS} \equiv \varepsilon_1(k=0)$] and the energy of the second band at the $k=0$ point just above the saddle point, i.e., $\varepsilon_2(k=0)$. The photon energy for the absorption peak seen in Fig. 2(f) would give $|\varepsilon_2(k=0) - \varepsilon_{\rm VHS}|$ and the values of μ at the first appearance and then disappearance of the peak would give $\varepsilon_{\rm VHS}$ and $\varepsilon_2(k=0)$, respectively, for a further check on the numbers.

In summary, we have examined the optical conductivity of twisted bilayer graphene using a simplified model for the low-energy band structure in order to bring out the qualitatively new features for this system. The monolayer graphene-like behavior at low energies that has been seen in STM measurements manifests itself in the conductivity as a flat universal background as a function of photon energy but with magnitude twice that of the monolayer. Finite doping introduces Pauli blocking in the band structure for interband transitions but spectral weight is transferred to a Drude response due to intraband processes. At higher energy, features analogous to unrotated bilayer graphene may be found but shifted in energy and different in origin. The saddle point between split Dirac cones in the band structure which is attributed to a VHS in the density of states, seen in STM, may be identified by the high-energy peak and the appearance of a new peak at low energy in the dynamical conductivity when the Fermi level sweeps through this region of the band structure. Thus, we provide a suggestion for a way to confirm the existence of this VHS through the spectroscopy of optical conductivity measurements, which may provide further confirmation of the existence of the unique band structure in twisted bilayer graphene that has been a source of dispute.

We thank J. P. Carbotte and P. San-Jose for helpful discussions. E.J.N. acknowledges the hospitality of the KITP, Santa Barbara. This work has been supported by NSERC of Canada and in part by the National Science Foundation under Grant No. NSF PHY11-25915.

[1] A. H. Castro Neto, F. Guinea, N. M. R. Peres, K. S. Novoselov, and A. K. Geim, Rev. Mod. Phys. **81**, 109 (2009).
[2] D. S. L. Abergel, V. Apalkov, J. Berashevich, K. Ziegler, and T. Chakraborty, Adv. Phys. **59**, 261 (2010).
[3] J. M. B. Lopes dos Santos, N. M. R. Peres, and A. H. Castro Neto, Phys. Rev. Lett. **99**, 256802 (2007).
[4] G. Li, A. Luican, J. L. dos Santos, A. C. Neto, A. Reina, J. Kong, and E. Andrei, Nat. Phys. **6**, 109 (2009).
[5] A. Luican, G. Li, A. Reina, J. Kong, R. R. Nair, K. S. Novoselov, A. K. Geim, and E. Y. Andrei, Phys. Rev. Lett. **106**, 126802 (2011).
[6] I. Brihuega, P. Mallet, H. Gonzalez-Herrero, G. T. de Laissardiere, M. Ugeda, L. Magaud, J. Gomez-Rodriguez, F. Yndurain, and J.-Y. Veuillen, Phys. Rev. Lett. **109**, 196802 (2012).
[7] G. Trambly de Laissardière, D. Mayou, and L. Magaud, Nano Lett. **10**, 804 (2010).
[8] P. San-Jose, J. González, and F. Guinea, Phys. Rev. Lett. **108**, 216802 (2012).
[9] R. Bistritzer and A. H. MacDonald, Proc. Nat. Acad. Sci. USA **108**, 12233 (2011).
[10] J. Hicks, M. Sprinkle, K. Shepperd, F. Wang, A. Tejeda, A. Taleb-Ibrahimi, F. Bertran, P. Le Fèvre, W. A. de Heer, C. Berger, and E. H. Conrad, Phys. Rev. B **83**, 205403 (2011).
[11] T. Ohta, J. T. Robinson, P. J. Feibelman, A. Bostwick, E. Rotenberg, and T. E. Beechem, Phys. Rev. Lett. **109**, 186807 (2012).
[12] R. de Gail, M. O. Goerbig, F. Guinea, G. Montambaux, and A. H. Castro Neto, Phys. Rev. B **84**, 045436 (2011).
[13] M.-Y. Choi, Y.-H. Hyun, and Y. Kim, Phys. Rev. B **84**, 195437 (2011).
[14] D. S. Lee, C. Riedl, T. Beringer, A. H. Castro Neto, K. von Klitzing, U. Starke, and J. H. Smet, Phys. Rev. Lett. **107**, 216602 (2011).
[15] K. Kim, S. Coh, L. Z. Tan, W. Regan, J. M. Yuk, E. Chatterjee, M. F. Crommie, M. L. Cohen, S. G. Louie, and A. Zettl, Phys. Rev. Lett. **108**, 246103 (2012).
[16] T. Ando, Y. Zheng, and H. Suzuura, J. Phys. Soc. Jpn. **71**, 1318 (2002).
[17] V. P. Gusynin and S. G. Sharapov, Phys. Rev. B **73**, 245411 (2006).
[18] V. P. Gusynin, S. G. Sharapov, and J. P. Carbotte, Phys. Rev. Lett. **96**, 256802 (2006).
[19] N. M. R. Peres, F. Guinea, and A. H. Castro Neto, Phys. Rev. B **73**, 125411 (2006).
[20] L. A. Falkovsky and A. A. Varlamov, Eur. Phys. J. B **56**, 281 (2007).
[21] T. Stauber, N. M. R. Peres, and A. H. Castro Neto, Phys. Rev. B **78**, 085418 (2008).
[22] D. S. L. Abergel and V. I. Fal'ko, Phys. Rev. B **75**, 155430 (2007).
[23] J. Nilsson, A. H. Castro Neto, F. Guinea, and N. M. R. Peres, Phys. Rev. B **78**, 045405 (2008).
[24] E. J. Nicol and J. P. Carbotte, Phys. Rev. B **77**, 155409 (2008).
[25] M. Koshino and T. Ando, Solid State Commun. **149**, 1123 (2009).
[26] L. M. Zhang, Z. Q. Li, D. N. Basov, M. M. Fogler, Z. Hao, and M. C. Martin, Phys. Rev. B **78**, 235408 (2008).
[27] Z. Q. Li, E. A. Henriksen, Z. Jiang, Z. Hao, M. C. Martin, P. Kim, H. L. Stormer, and D. N. Basov, Nat. Phys. **4**, 532 (2008).
[28] A. B. Kuzmenko, E. van Heumen, F. Carbone, and D. van der Marel, Phys. Rev. Lett. **100**, 117401 (2008).
[29] F. Wang, Y. Zhang, C. Tian, C. Girit, A. Zettl, M. Crommie, and Y. Shen, Science **320**, 206 (2008).

[30]R. R. Nair, B. Blake, A. N. Grigeronko, K. S. Novoselov, T. J. Booth, T. Stauber, N. M. R. Peres, and A. K. Geim, Science **320**, 1308 (2008).
[31]K. F. Mak, M. Y. Sfeir, Y. Wu, C. H. Lui, J. A. Misewich, and T. F. Heinz, Phys. Rev. Lett. **101**, 196405 (2008).
[32]Z. Q. Li, E. A. Henriksen, Z. Jiang, Z. Hao, M. C. Martin, P. Kim, H. L. Stormer, and D. N. Basov, Phys. Rev. Lett. **102**, 037403 (2009).
[33]A. B. Kuzmenko, E. van Heumen, D. van der Marel, P. Lerch, P. Blake, K. S. Novoselov, and A. K. Geim, Phys. Rev. B **79**, 115441 (2009).
[34]A. B. Kuzmenko, I. Crassee, D. van der Marel, P. Blake, and K. S. Novoselov, Phys. Rev. B **80**, 165406 (2009).
[35]M. Orlita and M. Potemski, Semicond. Sci. Technol. **25**, 063001 (2010).
[36]J. M. B. Lopes dos Santos, N. M. R. Peres, and A. H. Castro Neto, Phys. Rev. B **86**, 155449 (2012).
[37]E. J. Mele, J. Phys. D: Appl. Phys. **48**, 154004 (2012).
[38]E. J. Mele, Phys. Rev. B **81**, 161405 (2010).
[39]V. M. Apalkov and T. Chakraborty, Phys. Rev. B **84**, 033408 (2011).
[40]C. J. Tabert and E. J. Nicol, Phys. Rev. B **86**, 075439 (2012).
[41]G. D. Mahan, *Many Particle Physics* (Plenum, New York, 1990).
[42]L. Stille, C. J. Tabert, and E. J. Nicol, Phys. Rev. B **86**, 195405 (2012).
[43]T. Ohta, A. Bostwick, T. Seyller, K. Horn, and E. Rotenberg, Science **313**, 951 (2006).